International Research Journal of Innovations in Engineering and Technology (IRJIET)

ISSN (online): 2581-3048
Volume 6, Issue 10, pp 49-55, October-2022
https://doi.org/10.47001/IRJIET/2022.610008

Numerical Analysis of the Thermal-Hydraulic Performance on Circular Channel Using Vortex Generator

[1]M Iqbal Farhan Putra Arya, [2]Syaiful, [3]Muchammad

[1,2,3]Department of Mechanical Engineering, Faculty of Engineering, Diponegoro University, Semarang, Indonesia

***Abstract* - Vortex generators are often used in the industrial world because they can improve heat transfer well. Vortex generators make it possible to mix hot and cold fluids to be more optimal than not using them. Therefore, the current study aims to investigate the thermal-hydraulic of each case of a delta-winglet type vortex generator in a circular channel using numerical simulations. This modelling is carried out by varying the angle of the vortex generator type delta-winglet, namely, 90°, 105°, and 120°, which are arranged in a line, and the angle of attack in all cases is 30°. The Reynolds number is set from 4,000 to 12,000 with an interval of 2,000 and using the k-ω turbulent SST model. The working fluid used in this study is water. This fluid was chosen because it has better thermal conductivity than air, even though it has a higher viscosity and results in increased flow resistance. This study found that the highest heat transfer was a delta-winglet vortex generator at 90°, 105°, and 120°. But the delta-winglet, which has the highest heat transfer, will impact the increased flow resistance. Furthermore, the best thermal-hydraulic results were achieved in the case of the delta-winglet vortex generator at an angle of 120° of 2.47.**

Keywords: vortex generator, longitudinal vortex, heat transfer rate, friction factor, thermal-hydraulic.

I. INTRODUCTION

Improving the performance of heat exchangers in manufacturing and industry is very much needed to save energy [1-3]. In recent years, the industry has grown quite rapidly, such as in the food and beverages, pharmaceutical, and technical segments as in the current era. The allocation of place use for industry becomes a significant concentration for efficient production. Therefore, a heat exchanger with a more compact size and high performance is needed to solve current problems [4, 5]. And the present study helps study the efficiency improvement of the circular channel fitted by a delta-winglet type vortex generator (VG).

VG installations can disrupt the thermal boundary layer and have the effect of increasing heat transfer. There are several types of VG, including rectangular wing, delta wing, rectangular winglet, and delta winglet [6, 7]. The various VGs can be made by embossing, punching, stamping, and attaching [8]. Generally, VG produces a transverse or longitudinal vortex based on the surface type.

Promvonge and Skullong [9] investigated using VG rectangular winglets, and delta winglets with an angle of attack of 45° experimentally arranged in-line. The VG is placed in the middle of the circular channel on the top and flat bottom plates. Then, the Reynolds number was set at Re = 4.130 – 25.900 for research. The results of their study showed that the use of VG increased heat transfer higher than plain tubes. Moreover, the rectangular winglet vortex generator (RW VG) offers 6.05% better heat transfer than the delta winglet vortex generator (DW VG). However, the friction factor caused by the RW VG is more significant than the others. Subsequent research conducted by Sun et al. [10] identified the number of RW VGs placed around the circular channel experimentally and numerically. The number of RW VGs used is 4, 6, and 8. The results of their research show that the more number of VGs installed will increase the heat transfer highest than the others. Then, Liu et al. [11] analyzed heat transfer by installing RW VG in the center of the circular channel. The angle of attack of RW VG varied, respectively, from 10°, 20°, 30°, and 35°. The study's results found that in the case of RW VG, the angle of attack of 35° was the highest compared to the others when represented by the Nusselt number.

Liu et al. [12] studied improved heat transfer with and without a DW VG mounted around a fin-and-tube heat exchanger. The number of DW VG used is ten VG installed in the flow direction. Their study showed that the presence of DW VG induces secondary flow, which destroys the boundary layer and improves the heat transfer rate. Next, Oh and Kim [13] investigated the performance with various VG position and geometry effects. The VGs used are RW, delta-winglet upstream (DWU), and delta-winglet downstream (DWD), which are curved towards the fin-and-tube with position angles of 30°, 60°, 90°, and 105°, respectively. 120°, 135°, and 150°. This study found that the RW VG position angle of 135° produces higher secondary flow than the others, so the resulting heat transfer is also higher.

Based on previous studies, research by identifying thermal-hydraulic performance at variations in the DW VG

International Research Journal of Innovations in Engineering and Technology (IRJIET)

ISSN (online): 2581-3048

Volume 6, Issue 10, pp 49-55, October-2022

https://doi.org/10.47001/IRJIET/2022.610008

angle is still rarely done. Therefore, the current research seeks to identify and trace the heat transfer and flow resistance improvements present in each case. Then analyze the thermal-hydraulic performance of all cases by considering the Nusselt number and the friction factor.

II. MODEL DESCRIPTION

2.1 Physical Model

The present modelling uses circular channels and mounted VGs arranged in a line on a flat plate. A representative isometric scheme of mounting a flat plate with VG on a circular track can be seen in Figure 1. A DW VG was varied at 90°, 105°, and 120°, respectively, with the angle of attack set at 30°. The number of VGs installed along the channel is 56 pieces placed on the flat plate's top and bottom. The hydraulic diameter used in this channel is the diameter of the channel, which is 47 mm. Then, the longitudinal and latitudinal pitch distances between the VGs were 30 mm and 20 mm, respectively. This modelling refers to the numerical simulation done by Tian et al. [14]. Details of the implemented VG geometry variations can be seen in Figure 2 and Table 1. Furthermore, the working fluid used in this study is water with density, viscosity, heat capacity, and thermal conductivity, respectively 998.2 kg/m^3, 0.001003 kg/ms, 4.182 J/kgK, and 0.6 W/m^{2}K.

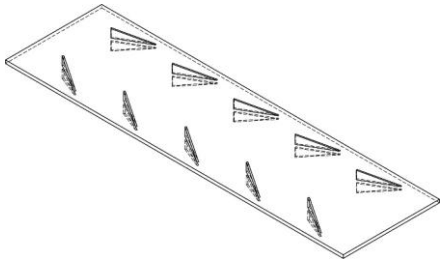

Figure 1: Isometric schematic of VG installation

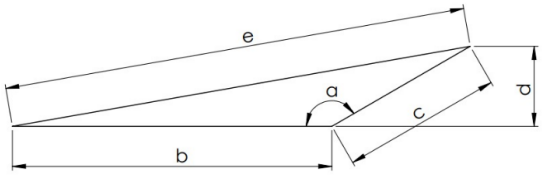

Figure 2: VG geometry

Table 1: DW VG side details

Angle of VG (α)	90°	105°	120°
Side (b)	16 mm	16 mm	16 mm
Side (c)	4 mm	4.14 mm	4.62 mm
Side (d)	4 mm	4 mm	4 mm
Side (e)	16. 49 mm	17.53 mm	18.74 mm

2.2 Governing Equations and Parameter Definitions

In this study, steady flow is assumed. Incompressible flow is also implemented along this circular channel. Furthermore, the winglets were also supposed to baffle walls with adiabatic conditions. Moreover, the pressure velocity coupling algorithm SIMPLE (Semi-Implicit Method for Pressure Linked Equations) with the viscous k-ω SST (Shear stress transport) model was considered to complete this research. Therefore, the equations used in this study, including the equations of continuity, momentum, energy conservation, and k-ω SST, can be stated as follows.

Continuity equation

$$\frac{\partial(\mathrm{R}\overline{\mathrm{u}_\mathrm{R}})}{\mathrm{R}}+\frac{\partial \mathrm{u}_\theta}{\mathrm{R}\partial\theta}+\frac{\partial \mathrm{u}_\mathrm{z}}{\partial \mathrm{z}}=0 \qquad (1)$$

Equation of momentum in the direction of R

$$\rho\left(\overline{\mathrm{u}_\mathrm{R}}\frac{\partial\overline{\mathrm{u}_\mathrm{R}}}{\partial \mathrm{R}}+\frac{\overline{\mathrm{u}_\theta}}{\theta}\frac{\partial\overline{\mathrm{u}_\mathrm{R}}}{\partial\theta}-\frac{\overline{\mathrm{u}_\theta}^2}{\mathrm{R}}+\overline{\mathrm{u}_\mathrm{z}}\frac{\partial\overline{\mathrm{u}_\mathrm{R}}}{\partial \mathrm{z}}\right) \qquad (2)$$
$$=-\frac{\partial\bar{\mathrm{p}}}{\partial \mathrm{R}}+\mu\left(\frac{1}{\mathrm{R}}\frac{\partial}{\partial \mathrm{R}}\left(\mathrm{R}\frac{\partial\overline{\mathrm{u}_\mathrm{R}}}{\mathrm{R}}\right)-\frac{\overline{\mathrm{u}_\mathrm{R}}}{\mathrm{R}^2}+\frac{\partial^2\overline{\mathrm{u}_\mathrm{R}}}{\mathrm{R}^2\partial\theta^2}-\frac{2}{\mathrm{R}^2}\frac{\partial\overline{\mathrm{u}_\theta}}{\partial\theta}+\frac{\partial^2\overline{\mathrm{u}_\mathrm{R}}}{\partial \mathrm{z}^2}\right)+\frac{\partial}{\partial\theta}\left(-\rho\overline{\mathrm{u}_\mathrm{R}'\mathrm{u}_\theta'}\right)+\frac{\partial}{\partial \mathrm{z}}\left(-\rho\overline{\mathrm{u}_\mathrm{R}'\mathrm{u}_\mathrm{z}'}\right)$$

Equation of momentum in the direction of θ

$$\rho\left(\overline{\mathrm{u}_\mathrm{R}}\frac{\partial\overline{\mathrm{u}_\theta}}{\partial \mathrm{R}}+\frac{\overline{\mathrm{u}_\theta}}{\mathrm{R}}\frac{\partial\overline{\mathrm{u}_\theta}}{\partial\theta}-\frac{\overline{\mathrm{u}_\theta\mathrm{u}_\mathrm{R}}}{\mathrm{R}}+\overline{\mathrm{u}_\mathrm{z}}\frac{\partial\overline{\mathrm{u}_\theta}}{\partial \mathrm{z}}\right) \qquad (3)$$
$$=-\frac{\partial\bar{\mathrm{p}}}{\mathrm{R}\partial\theta}+\mu\left(\frac{1}{\mathrm{R}}\frac{\partial}{\partial \mathrm{R}}\left(\mathrm{R}\frac{\partial\overline{\mathrm{u}_\theta}}{\partial \mathrm{R}}\right)-\frac{\overline{\mathrm{u}_\theta}}{\mathrm{R}^2}+\frac{\partial^2\overline{\mathrm{u}_\theta}}{\mathrm{R}^2\partial\theta^2}-\frac{2}{\mathrm{R}^2}\frac{\partial\overline{\mathrm{u}_\mathrm{R}}}{\partial\theta}+\frac{\partial^2\overline{\mathrm{u}_\theta}}{\partial \mathrm{z}^2}\right)+\frac{\partial}{\partial \mathrm{R}}\left(-\rho\overline{\mathrm{u}_\theta'\mathrm{u}_\mathrm{R}'}\right)+\frac{\partial}{\partial \mathrm{z}}\left(-\rho\overline{\mathrm{u}_\theta'\mathrm{u}_\mathrm{z}'}\right)$$

Equation of momentum in the direction of z

$$\rho\left(\overline{\mathrm{u}_\mathrm{R}}\frac{\partial\overline{\mathrm{u}_\mathrm{z}}}{\partial \mathrm{R}}+\frac{\overline{\mathrm{u}_\theta}}{\mathrm{R}}\frac{\partial\overline{\mathrm{u}_\mathrm{z}}}{\partial\theta}+\overline{\mathrm{u}_\mathrm{z}}\frac{\partial\overline{\mathrm{u}_\theta}}{\partial \mathrm{z}}\right) \qquad (4)$$
$$=-\frac{\partial\bar{\mathrm{p}}}{\partial Z}+\mu\left(\frac{1}{\mathrm{R}}\frac{\partial}{\partial \mathrm{R}}\left(\mathrm{R}\frac{\partial\overline{\mathrm{u}_\mathrm{z}}}{\partial \mathrm{R}}\right)+\frac{\partial^2\overline{\mathrm{u}_\mathrm{z}}}{\mathrm{R}^2\partial\theta^2}+\frac{\partial^2\overline{\mathrm{u}_\mathrm{z}}}{\partial \mathrm{z}^2}\right)+\frac{\partial}{\partial \mathrm{R}}\left(-\rho\overline{\mathrm{u}_\mathrm{z}'\mathrm{u}_\mathrm{R}'}\right)+\frac{\partial}{\partial\theta}\left(-\rho\overline{\mathrm{u}_\theta'\mathrm{u}_\mathrm{z}'}\right)$$

International Research Journal of Innovations in Engineering and Technology (IRJIET)

ISSN (online): 2581-3048

Volume 6, Issue 10, pp 49-55, October-2022

https://doi.org/10.47001/IRJIET/2022.610008

Transport equation for k-ω SST

$$\frac{\partial}{\partial t}(\rho k) + \frac{\partial}{\partial x_i}(\rho k u_i) = \left(\Gamma_k \frac{\partial k}{\partial x_j}\right) + \bar{G}_k - Y_k + S_k \quad (5)$$

$$\frac{\partial}{\partial t}(\rho \omega) + \frac{\partial}{\partial x_i}(\rho \omega u_i) = \frac{\partial}{\partial x_j}\left(\Gamma_\omega \frac{\partial \omega}{\partial x_j}\right) + \bar{G}_\omega - Y_\omega + D_\omega + S_\omega \quad (6)$$

Energy conservation

$$\rho C_P \left(u_R \frac{\partial T}{\partial R} + \frac{u_\theta}{R}\frac{\partial T}{\partial \theta} + u_z \frac{\partial T}{\partial z}\right) = -\lambda\left(\frac{1}{R}\frac{\partial}{\partial R}\left(R\frac{\partial T}{\partial R}\right) + \frac{1}{R^2}\frac{\partial^2 T}{\partial \theta^2} + \frac{\partial^2 T}{\partial z^2}\right) \quad (7)$$

This study will also examine the thermal-hydraulic performance with TEF (Thermal Enhancement Factor), which is sought by identifying the Reynolds number, Nusselt number, and friction factor.

Reynolds number

$$Re = \frac{\rho \bar{v} D_h}{\mu} \quad (8)$$

Nusselt number

$$Nu = \frac{h D_h}{\lambda} \quad (9)$$

Friction factor

$$f = \frac{\Delta P D_h}{\frac{1}{2}\rho u^2 L} \quad (10)$$

Where, ρ, $\bar{v}$, D_h, μ, λ, and Lare density, intake air flow velocity, hydraulic diameter, dynamic viscosity, thermal conductivity of air, and line length, respectively.

Thermal enhancement factor (TEF)

$$TEF = \frac{\frac{\overline{Nu}}{\overline{Nu_0}}}{\left(\frac{f}{f_0}\right)^{\frac{1}{3}}} \quad (11)$$

Where, subscript 0 is the plane tube condition (without VG).

2.3 Computational domain and boundary conditions

Figure 3 shows the computational domain of a circular channel fitted with a flat plate with VG. In this domain, the X and Y axes indicate the flow and cross-flow directions, respectively. To ensure that the flow that enters the test section is uniform, the computational domain is extended half the length of the test section. Furthermore, if the flow out of the test section is extended five times compared to that of the test section, it is helpful to prevent reverse flow along the flow.

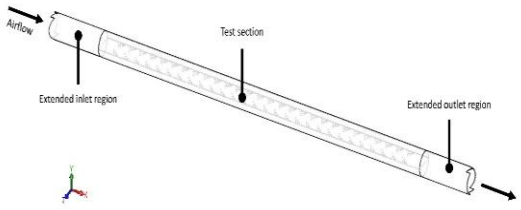

Figure 3: Computational domain

The boundary conditions used in this study are inlet, outlet, and wall conditions, which are the conditions specified in the initial initialization of this numerical simulation study respectively. Following are the implemented boundary conditions.

Inlet

$$u_z = u_{z,\,in};\ u_\theta = u_R = 0;\ p = p_{in};\ T_{in} = 300K \quad (12)$$

Wall

$$T_w = 500K \quad (13)$$

Outlet

$$\frac{\partial u_z}{\partial z} = 0;\ \frac{\partial p}{\partial z} = 0;\ \frac{\partial T}{\partial z} = 0 \quad (14)$$

2.4 Grid Independence Test

ANSYS Fluent is used to produce the optimum grid structure. The mesh topology used is polyhedral. This is because the shape has more sides so that it can speed up calculations on fairly complex geometries [15]. Figure 4 shows the mesh structure of two vortex generators arranged at the top and bottom of the flat plate. It can be seen that the mesh has inflation on each side and has an impact on the more accurate results of numerical simulations on geometries that tend to have a narrower surface area. This meshing test was carried out on the delta-winglet VG geometry, which has the most significant angle, and the Reynolds number is set at Re = 12,000. The results of the grid independent test of this study found that 1.8 million is the optimum grid and were chosen to solve problems in other cases. More details can be seen in Figure 5.

International Research Journal of Innovations in Engineering and Technology (IRJIET)

ISSN (online): 2581-3048

Volume 6, Issue 10, pp 49-55, October-2022

https://doi.org/10.47001/IRJIET/2022.610008

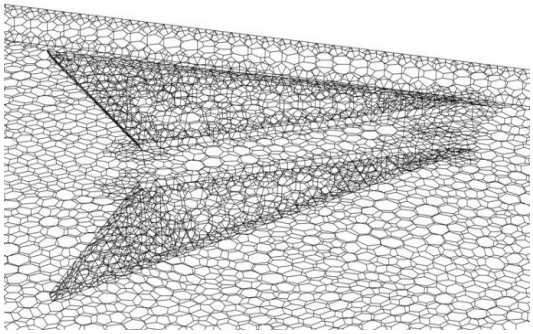

Figure 4: Detail polyhedral mesh

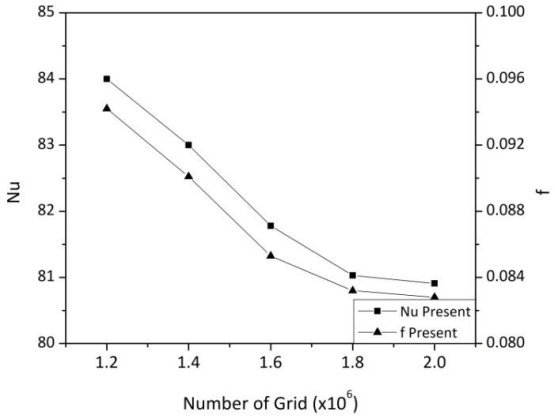

Figure 5: Grid independence test

III. NUMERICAL METHOD AND VALIDATION

This study was completed using the SIMPLE algorithm and a pressure-velocity coupling model of turbulent k-ω SST (Shear Stress Transport). This modelling also uses a second-order upwind scheme approach to solve the momentum, pressure, and energy equations. Then, the validation used in this study is a comparison between the numerical simulation of this study with the Dittus-Boelter and Blasius correlations for the Nusselt number and the friction factor, respectively. It is used to compare the results of heat transfer and flow resistance in the pipe channel without plates or turbulators. The error deviation in this study is 3.58%, and can be seen in Figure 6.

Dittus-Boelter correlation

$$Nu_D = 0.023\, Re_D^{0.8} Pr^{0.4} \qquad (15)$$

Where Nu, Re, and Pr are Nusselt numbers, Reynolds numbers, and Prandtl numbers, respectively.

Blasius correlation

$$f_B = 0.316\, Re^{0.25} \qquad (16)$$

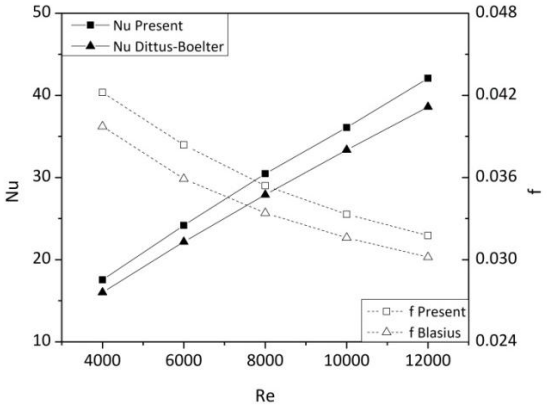

Figure 6: Circular channel modeling validation

IV. RESULT AND DISCUSSION

4.1 Heat Transfer and Temperature Distribution

Figure 7 shows the graph between the Reynolds number and the Nusselt number for all variations of the DW VG angle. Overall, the results from each case have a similar tendency, but it is seen that the 90° DW VG angle has the highest and most impressive Nusselt number at Re = 12,000.

However, at the Reynolds number below, each VG has no difference, even though the 90° DW VG angle still has the best heat transfer improvement. When compared at Re = 12,000, the Nusselt number of the 90° angle DW VG is higher than that of the 105° angle and the 120° angle, 0.79% and 1.19%, respectively. This shows that the same VG surface area but different angles can affect the mixing of hot and cold fluids and impact different heat transfer improvements. Moreover, the higher the Reynolds number, the higher the Nusselt number because of the influence of the convection coefficient in each case [16].

The temperature distribution in Figure 8 is presented to strengthen the previous data. In all cases, the contours were taken on the YZ plane at location X = 900 mm. Seen in the picture has a similar tendency, although the temperature appears to be different.

When analyzed from the three images, the 90° DW VG angle indicates a higher tangential velocity vector than the other cases, which is indicated by a larger arrow than the others. Then, for the DW VG angle of 120°, it is also seen that the mixing of hot and cold fluids is not evenly distributed, so the heat transfer is less than optimal [17].

ISSN (online): 2581-3048
Volume 6, Issue 10, pp 49-55, October-2022
https://doi.org/10.47001/IRJIET/2022.610008

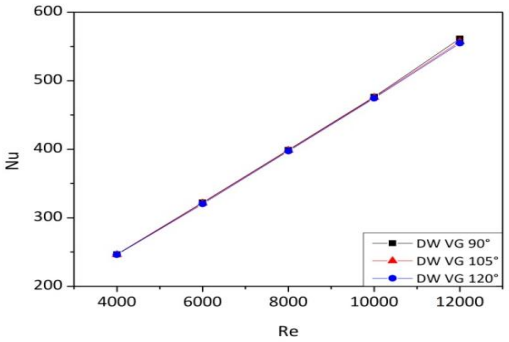

Figure 7: Nusselt number variation with the Reynolds number at different angle of DW VG

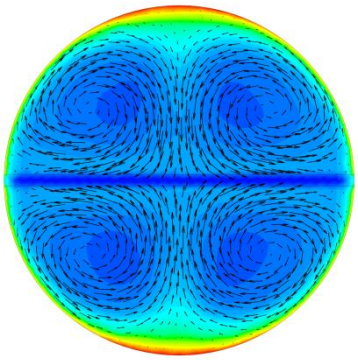

(a)

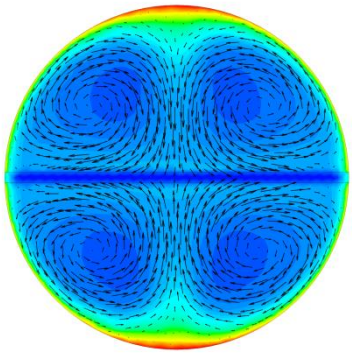

(b)

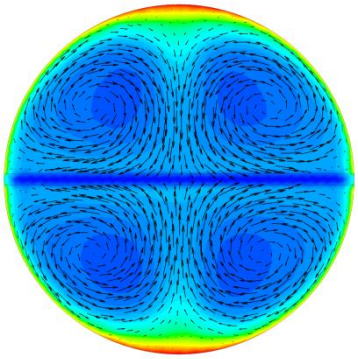

(c)

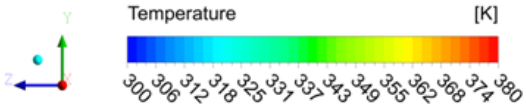

Figure 8: Temperature contours in the YZ plane in each case VG (a) 90°, (b) 105°, and (c) 120°

4.2 Flow Resistance and Pressure Drop

Figure 9 shows a graph between the Reynolds number and friction factor in each case from Re = 4,000 to Re = 12,000. The figure found that the higher the Reynolds number, the lower the friction factor value. This is because the flow resistance at the lowest Reynolds number is higher than that at the highest Reynolds number. All analyzed DW VG cases showed a similar tendency. The 120° DW VG angle has the lowest friction factor of the others. When compared between a 120° DW VG angle and a 105° or 90° DW VG angle, the 120° DW VG angle has a reduction in friction factor of 1.78% and 3.49%, respectively.

Figure 10 shows that the highest-pressure difference is obtained in the cases of DW VG angle of 90°, DW VG angle of 105°, and DW VG angle of 120°. This is directly proportional to the temperature contour in Figure 8. This shows the magnitude of the tangential velocity at 90° DW VG causing a high-pressure drop in this case. It may also be possible because of the longitudinal vortex (LV), which affects the pressure drop along the flow [18].

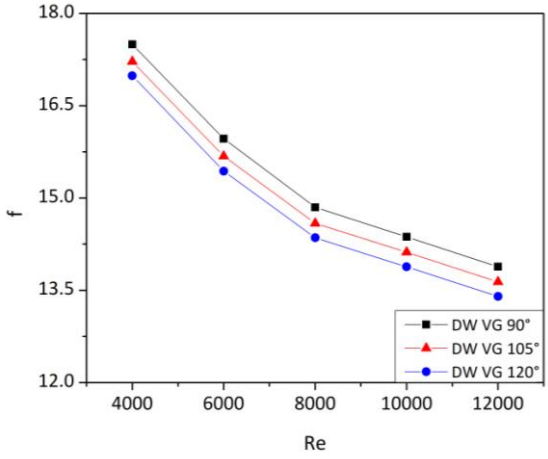

Figure 9: Friction factor variation with the Reynolds number at different angle of DW VG

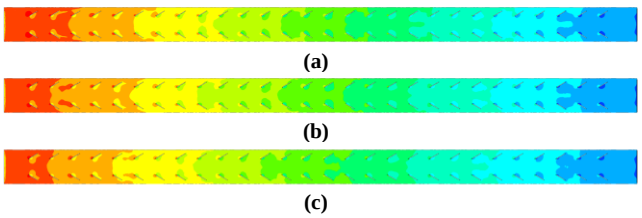

(a)

(b)

(c)

ISSN (online): 2581-3048
Volume 6, Issue 10, pp 49-55, October-2022
https://doi.org/10.47001/IRJIET/2022.610008

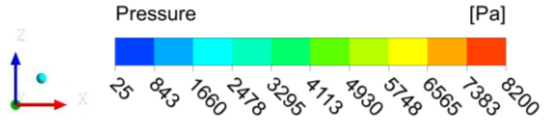

Figure 10: Pressure contours of the ZX plane at Y = 1.5 mm in each case VG (a) 90°, (b) 105°, and (c) 120°

4.3 Thermal-hydraulic performance

The way to determine the thermal-hydraulic performance of this study is to use the TEF parameter. TEF is calculated by comparing the Nusselt number ratio and friction factor in each case in this study [19, 20]. The best performance is the case with a higher TEF than the others. This can be seen in the DW VG angle of 120°, which has the highest TEF. This is because the increase in the Nusselt number is higher than the increase in the friction factor. In other words, the heat transfer rate is higher than the resistance to flow. At Re = 6,000, it was found that the TEF value was not significant because it was estimated that the value of the Nusselt number tended not to increase more than Re = 4,000. Moreover, at Re = 10,000, the gap between each case is 2.33, 2.34, and 2.36, respectively. Figure 10 Pressure contours of the ZX plane at Y = 1.5 mm in each case VG (a) 90°, (b) 105°, and (c) 120°.

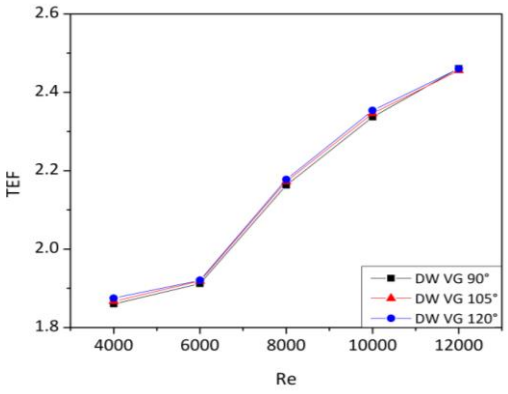

Figure 11: TEF variation with the Reynolds number at different angle of DW VG

V. CONCLUSION

The current study helps determine the thermal-hydraulic performance with DW VG installation in circular channels. The variation in this study is the difference in angles in DW VG, which are 90°, 105°, and 120° with Reynolds number 4,000 to 12,000 with an interval of 2,000. The results of this numerical simulation can be concluded as follows.

1. The highest increase in heat transfer indicated by the Nusselt number is in the case of DW VG 90°. This is due to the high tangential velocity at the back cross-section of the test resulting in a more optimal mixing of hot and cold fluids.
2. The highest friction factor was found at Re = 4,000 in the case of DW VG 90° worth 17.49. At the same time, the value of the friction factor tends to decrease when the Reynolds number increases. So, at Re = 12,000 in the case of DW VG 90°, it becomes 13.88.
3. The best performance of all cases studied was found in the case of DW VG 120°. This is indicated because the increase in heat transfer tends to be higher than the friction factor.

ACKNOWLEDGEMENT

The researchers would like to thank the all member of Thermo fluid Laboratory, Mechanical Engineering Department at the Diponegoro University. Also, thanks for supporting us.

REFERENCES

[1] J. Li, C. Dang, and E. Hihara, "Heat transfer enhancement in a parallel, finless heat exchanger using a longitudinal vortex generator, Part A: Numerical investigation," *International Journal of Heat and Mass Transfer*, vol. 128, pp. 87-97, 2019.

[2] Z. Han, Z. Xu, and H. Qu, "Parametric study of the particulate fouling characteristics of vortex generators in a heat exchanger," *Applied Thermal Engineering*, vol. 167, pp. 114735, 2020.

[3] W. A. Abdelmaksoud, A. E. Mahfouz, and E. E. Khalil, "Thermal Performance Enhancement for Heat Exchanger Tube Fitted with Vortex Generator Inserts," *Heat Transfer Engineering*, vol. 42, pp. 1861-1875, 2021.

[4] A. J. Modi, N. A. Kalel,and M. K. Rathod, "Thermal performance augmentation of fin-and-tube heat exchanger using rectangular winglet vortex generators having circular punched holes," *International Journal of Heat and Mass Transfer*, vol. 158, pp. 119724, 2020.

[5] A. A. Gholami, M. A. Wahid, and H. A. Mohammed, "Heat transfer enhancement and pressure drop for fin-and-tube compact heat exchangers with wavy rectangular winglet-type vortex generators," *International Communications in Heat and Mass Transfer*, vol. 54, pp. 132-140, 2014.

[6] A. M. Jacobi and R. K. Shah, "Heat transfer surface enhancement through the use of longitudinal vortices: A review of recent progress," *Experimental Thermal and Fluid Science*, vol. 11, pp. 295-309, 1995.

[7] H. E. Ahmed, H. A. Mohammed, and M. Z., Yusoff, "An overview on heat transfer augmentation using vortex generators and nanofluids: Approaches and applications," *Renewable and Sustainable Energy Reviews*, vol. 16, pp. 5951-5993, 2012.

ISSN (online): 2581-3048
Volume 6, Issue 10, pp 49-55, October-2022
https://doi.org/10.47001/IRJIET/2022.610008

[8] M. Fiebiq and Y. Chen, "Heat Transfer Enhancement by Wing-Type Longitudinal Vortex Generators and their Application to Finned Oval Tube Heat Exchanger Elements," *Heat Transfer Enhancement of Heat Exchangers*, vol. 355, pp. 79-105, 1999.

[9] P. Promvonge and S. Skullong, "Thermo-hydraulic performance in heat exchanger tube with V-shaped winglet vortex generator," *Applied Thermal Engineering*, vol. 164, pp. 114424, 2020.

[10] Z. Sun, K. Zhang, W. Li, Q. Chen, and N. Zhen, "Investigations of the turbulent thermal-hydraulic performance in circular heat exchanger tubes with multiple rectangular winglet vortex generators," *Applied Thermal Engineering*, vol. 168, pp. 114838, 2020.

[11] H. L. Liu, H. Li, Y. L. He, and Z. T. Chen, "Heat transfer and flow characteristics in a circular tube fitted with rectangular winglet vortex generators," *International Journal of Heat and Mass Transfer*, vol. 126A, pp. 989-1006, 2018.

[12] Y. Liu, X. Ma, X. Ye, Y. Chen, Y. Cheng, and Z. Lan, "Heat transfer enhancement of annular finned tube exchanger using vortex generators: The effect of oriented functional circumferential arrangement," *Thermal Science and Engineering Progress*, vol. 10, pp. 27-35, 2019.

[13] Y. Oh and K. Kim, "Effects of position and geometry of curved vortex generators on fin-tube heat-exchanger performance characteristics," *Applied Thermal Engineering*, vol. 189, pp. 116736, 2021.

[14] M. W. Tian, S. Khorasani, H. Moria, S. Pourhedayat, and H. S. Dizaji, "Profit and efficiency boost of triangular vortex-generators by novel techniques," *International Journal of Heat and Mass Transfer*, vol. 156, pp. 119842, 2020.

[15] Syaiful, T. A. Wicaksono, M. S. K. Tony, A. Suprihanto, and M. F. Soetanto, "Heat transfer intensification with field synergy principle in a fin-and-tube heat exchanger through convex strip installation," *Engineering Reports*, vol. 4, pp. 1-26, 2022.

[16] A. U. Tepe, "Heat transfer enhancement of fin-tube heat exchangers using punched triangular ramp vortex generator on the fin surface," *International Journal of Heat and Mass Transfer*, vol. 174, pp. 121326, 2021.

[17] K. S. Rambhad, V. P. Kalbande, M. A. Kumbhalkar, V. W. Khond, and R. A. Jibhakate, "Heat Transfer and Fluid Flow Analysis for Turbulent Flow in Circular Pipe with Vortex Generator," *SN Applied Sciences*, vol. 3, pp. 1-21, 2021.

[18] S. K. Sarangi, N. Anand, K. Srivastava, P. Chamoli, D. P. Mishra, and L. S. Brar, "Heat Transfer and Pressure Drop Assessment of a Vortex Generator Supported Fin-And-Tube Heat Exchanger," *Advances in Mechanical Processing and Design*, vol. 1, pp. 149-159, 2020.

[19] N. Zheng, K. Zhang, Q. Chen, and Z. Sun, "Novel self-join winglet vortex generators for enhanced heat transfer of turbulent airflow in round tubes," *International Communications in Heat and Mass Transfer*, vol. 130, pp. 105806, 2022.

[20] Z. Zhao, L. Luo, D. Qiu, Z. Wang, and B. Sunden, "On the solar air heater thermal enhancement and flow topology using differently shaped ribs combined with delta-winglet vortex generators," *Energy*, vol. 224, pp. 119944, 2021.

Citation of this Article:

M Iqbal Farhan Putra Arya, Syaiful, Muchammad, "Numerical Analysis of the Thermal-Hydraulic Performance on Circular Channel Using Vortex Generator" Published in *International Research Journal of Innovations in Engineering and Technology - IRJIET*, Volume 6, Issue 10, pp 49-55, October 2022. Article DOI https://doi.org/10.47001/IRJIET/2022.610008

****

